ACS Photonics

pubs.acs.org/journal/apchd5

Article

Relaxing Symmetry Rules for Nonlinear Optical Interactions in Van der Waals Materials via Strong Light–Matter Coupling

Mandeep Khatoniar, Rezlind Bushati, Ahmed Mekawy, Florian Dirnberger, Andrea Alù, and Vinod M Menon*

Cite This: *ACS Photonics* 2022, 9, 503–510

Read Online

ACCESS | Metrics & More | Article Recommendations | Supporting Information

ABSTRACT: Transition metal dichalcogenides (TMDCs) have been in the limelight for the past decade as a candidate for several optoelectronic devices and as a versatile test bed for various fundamental light–matter interaction phenomena thanks to their exceptional linear optical properties arising from their large binding energy, strong spin–orbit coupling, and valley physics in the monolayer (ML) limit. They also boast strong nonlinear properties fortified by excitonic responses in these systems. However, the strong second-order nonlinear responses are mostly restricted to the ML limit, owing to crystal symmetry requirements, posing several limitations in terms of smaller interaction length and lower damage threshold. Here we demonstrate a self-hybridized exciton–polariton system in bulk WSe_2 that allows us to relax the crystal symmetry rules that govern second-order nonlinearities. The demonstrated polariton system shows intense second harmonic generation (SHG) when the fundamental wavelength is resonant with the lower polariton, with an efficiency comparable to the one from a ML WS_2 when excited at the same fundamental wavelength and intensity. We model this phenomenon by considering a system with alternating second-order susceptibilities under an asymmetric electric field profile determined by the polariton mode. Helicity-resolved polarization experiments show a very similar nonlinear response as the one from a ML, where the helicity of the SHG flips with respect to the fundamental harmonic. This polaritonic system offers a platform to leverage a robust second-order nonlinear response from centrosymmetric systems, while at the same time allowing access to third-order nonlinearity inherent in strongly coupled systems.

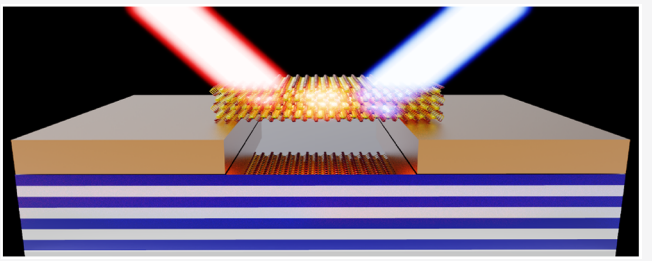

KEYWORDS: *exciton–polaritons, self-hybridization, TMDC, nonlinear optics, second-harmonic generation, strong light–matter interactions*

Transition metal dichalcogenides (TMDCs) are van der Waals (vdW) materials that exhibit a vista of much sought after optical and electronic properties. They have been studied extensively in the monolayer (ML) limit due to their direct bandgap, large exciton binding energy, valley properties, and oscillator strength.[1−4] Due to these properties, strong coupling between cavity photons in microcavities and excitons in ML TMDCs can be demonstrated at room temperature.[5] In addtion in such a strongly coupled system, the polaritons retain the valley excitonic properties of the host material.[6−8] More recently, there has been interest in polaritons formed in bulk TMDCs due to their high refractive index, which enables Fabry–Perot modes to be sustained in TMDC slabs that strongly couple with the exciton modes of the bulk TMDC.[9−11] This coupling results in a self-hybridized system, where the bulk TMDC itself provides both the photonic and the excitonic components required for strong coupling, without the need for an external cavity.

In addition to their exceptional linear optical properties, there have also been numerous reports on their nonlinear optical response. Second harmonic generation (SHG) can be observed in TMDCs owing to the lack of inversion symmetry in the ML and odd layer limit.[12−15] More recently, SHG in TMDCs has emerged as a powerful spectroscopic tool to characterize the layer number as well as the crystal orientation, the latter being an important parameter for achieving a precise twist angle in vdW heterostructures.[16−19] In addition to intense SHG, other second-order susceptibility $\chi^{(2)}$-mediated processes like sum frequency generation at continuous wave pump, optical parametric amplification, and signatures of spontaneous parametric down-conversion have also been realized in these systems.[20−22] These nonlinear optical responses can be further enhanced by engineering light–matter interactions with nanophotonic tools. Since 2D TMDCs show high values of nonlinear susceptibility (e.g.,

Received: August 16, 2021
Published: January 26, 2022

two-photon absorption in MoS_2 is 4 orders of magnitude larger than III−V group semiconductors such as GaAs), they represent an ideal system for nonlinear optical applications.[23] Despite this advantage, 2D TMDCs suffer from the limitation that the second-order nonlinear response is limited to the ML/odd few layer limit, which proves to be a challenge for device integration. Several attempts have been put forward to increase the interaction time via auxiliary systems where ML or few-layer TMDCs couple to plasmonic or photonic modes in passive[24−27] or active[28] nanostructures.

The restoration of inversion symmetry in bulk TMDC crystals with naturally occurring 2H stacking prohibits second-order nonlinearity under the electric dipole approximation, consequently creating a limitation in terms of the available interaction length. Several attempts to amplify weak $\chi^{(2)}$ in centrosymmetric silicon via geometric structuring that invokes effects beyond the dipole approximation, or amplification of weak surface $\chi^{(2)}$ via integration with large quality factor photonic modes, have been demonstrated.[29−32] In addition to feeble responses, these practices suffer from stringent resonance requirements that cause a bottleneck in terms of fabrication and integration. In this work, we achieve a strong nonlinear $\chi^{(2)}$ response, despite the presence of inversion symmetry, in planar self-hybridized exciton−polaritons formed via strong coupling of Fabry−Perot modes sustained by bulk (140 nm) WSe_2 and the exciton resonances of each layer. The existence of these modes creates a nonzero phase difference between the SHG signal generated in each layer, owing to the asymmetry of the electric field of the fundamental laser at the polariton mode, which when added coherently, does not cancel out in the far field. Recently, SHG from patterned bulk TMD has been shown in ref 28, where flakes of a certain thickness were preselected based on the weak SHG signal in their bulk form. In contrast, our approach eliminates stringent thickness requirements and also provides an insight into the details of the SHG process. We compare the polarization responses of this polariton system and find they exhibit similar behavior as their ML counterparts. A comparison between a ML TMDC system and these self-hybridized polariton systems show that the latter is more efficient at lower powers than the former. The strong coupling-assisted approach presented here allows to simultaneously use material systems where crystal symmetry-dependent selection rules can be relaxed to recover latent nonlinearity while leveraging the additional photonic control knobs and the inherent nonlinearity of polariton fluids.[33] Along with their facile "pick and place" fabrication, this platform offers relatively broadband responses, thus, making it an attractive candidate for the realization of nonlinear photonics applications.

RESULTS

Figure 1a shows the schematic of the structure used in this work, which consists of a bulk dry WSe_2 flake transferred on top of a 7.5 μm^2 square box that was etched on a 10.5 period distributed Bragg reflector (DBR) consisting of alternating TiO_2/SiO_2 layers. The thickness of the bulk TMDC and the depth of the square hole were optimized using transfer matrix calculations and coupled mode theory such that self-hybridized exciton−polaritons are only formed within the square structure, and outside the etched box there are no polaritons supported. This step ensures homogeneity of the refractive index surrounding region in which polaritons are formed. Moreover, a single flake can host both the regions of polariton

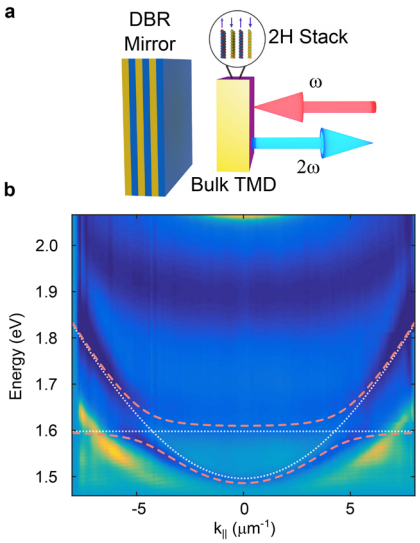

Figure 1. (a) Schematic of the WSe_2 polariton device. (b) White light spectrum of the polariton system and a coupled oscillator model fit used to extract the polariton parameters shown in pink dashed lines.

formation as well as a reference region with no strong coupling. See Methods for details. Figure 1b shows the white light reflection taken at the location of the square box, indicating the presence of two new eigenmodes, namely, the upper and the lower polariton branches. We fit a coupled oscillator model to obtain a Rabi splitting of 70 meV and a negative cavity mode detuning of 77.5 meV. Transfer matrix simulation and experimental data for the white light reflection spectrum taken outside the square region are shown in Figure S1.

Figure 2a shows the SHG signal (in blue) when the lower polariton is excited with a pulsed Ti:sapphire laser tuned at a wavelength resonant to the minima of the lower polariton branch (at $k_{\parallel} = 0$). As a comparison, the SHG signal from the region where no polaritons are formed (outside the square) is also shown in Figure 2a (in red). A sharp signal at half the wavelength of the fundamental is observed in the case of resonant excitation of the polariton branch. The output intensity versus input power dependence in logarithmic scale is plotted in Figure S2a, which shows a slope of 1.83, which is indicative of SHG. We detect no discernible signal from the region outside the square box and estimate a lower bound for the enhancement factor based on the detector noise levels. Inside the box, the SHG signal is enhanced at least by 3 orders of magnitude. Figure 2b compares the SHG intensity as a function of detuning of the fundamental wavelength λ_F from the one at $k_{\parallel} = 0$, λ_0. The laser has a line width of approximately 4.3 nm, and the polariton line width is 20 nm. We find that the SHG signal is reduced by 80% for a laser-cavity detuning of 15 nm.

To further characterize the nature of the SHG in the polariton system, we resort to polarization-dependent studies. We measure the linear polarization response of the SHG by rotating the plane of input linear polarization of the fundamental while keeping the bulk TMDC and an output analyzer stationary. Under this measurement configuration, the D_3h symmetry structure should give a 4-fold symmetry.[34] See Supporting Information, Note 3 for details. The inset of Figure 3a shows the 4-fold symmetry as a function of the input polarization of the fundamental excitation. This gives distinctive evidence that the SHG originates from a crystal

https://doi.org/10.1021/acsphotonics.1c01242
ACS Photonics 2022, 9, 503−510

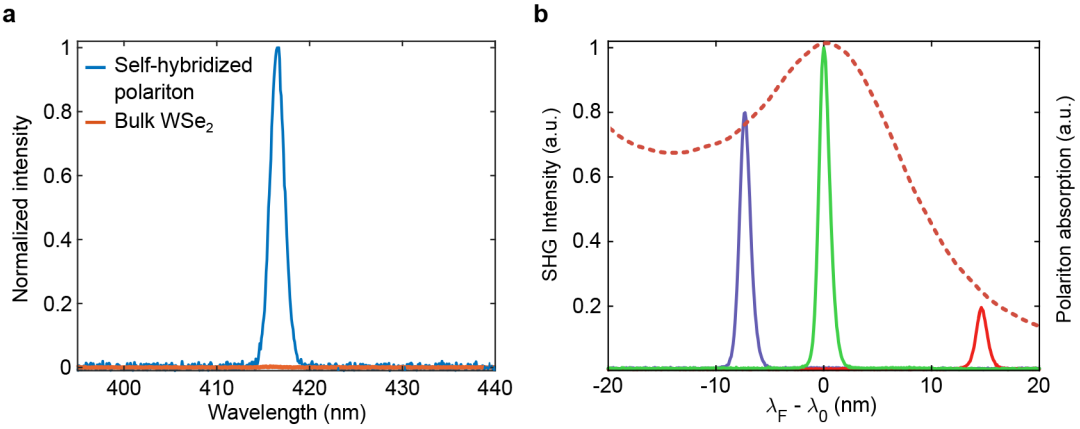

Figure 2. (a) SHG response of the polariton device with the fundamental resonant with a wavelength at $k_{\|} = 0$. (b) Comparison of the relative SHG intensity as a function of detuning of the fundamental (λ_F) laser from the peak wavelength at $k_{\|} = 0$ (λ_0). The red dotted curve is the line cut of the polariton branch at $k_{\|} = 0$. The blue, green, and red curves are the SHG intensities at $-ve$, 0, and $+ve$ detuning, respectively.

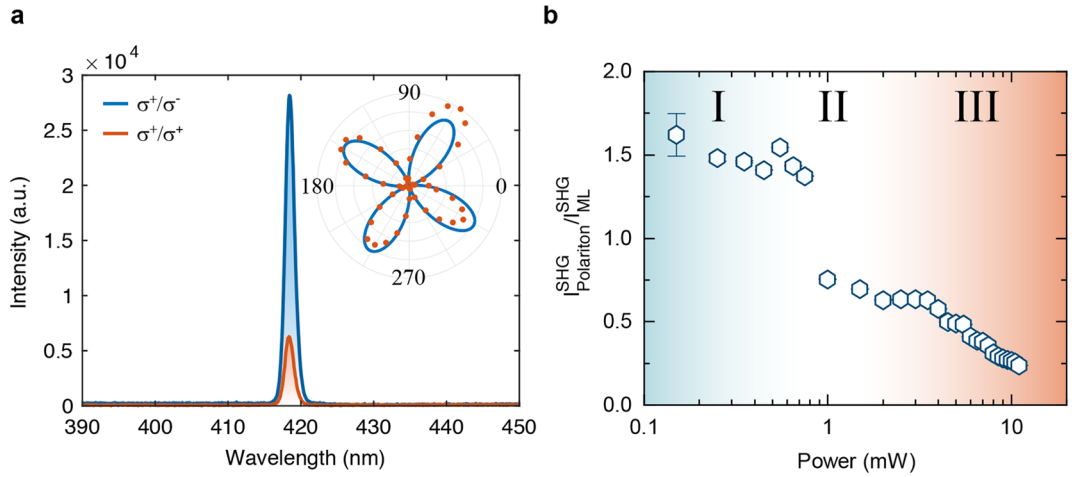

Figure 3. (a) SHG response as a function of input circular polarization. The helicity of the SHG is flipped as seen in ML systems. Inset shows the SHG response as a function of input linear polarization for a fixed analyzer. (b) The ratio of SHG intensity of a polariton system and a ML WS_2 pumped at the same fundamental wavelength. Error bars represent fitting errors while extracting the area under the curve of the SHG signals.

with a D_3h symmetry group, and it can be attributed to the residual phase that the SHG and the fundamental pick up due to multiple reflections within the structure, thereby producing a nonzero SHG in the far field. After confirming the crystal symmetry, we excite the sample with a circularly polarized fundamental. As seen in ML TMDCs, the polariton system also produces a circularly polarized SHG signal. Figure 3a shows that the measured SHG signal when excited with σ^+ fundamental. The helicity of the SHG signal is flipped from the one of the fundamental, thereby confirming the D_3h symmetry.[35] We define degree of circular polarization as $\rho = \left|\frac{I^{\sigma^+} - I^{\sigma^-}}{I^{\sigma^+} + I^{\sigma^-}}\right|$, where I^{σ^+} is the intensity of the right-handed circularly polarized light and I^{σ^-} is the intensity of left-handed circularly polarized light when analyzed through a quarter wave plate and linear polarizer at the output. After normalizing with the degree of circular polarization of the laser, we obtain a value of $\rho = 0.87$ for the case of bulk WSe_2 polaritons, which is comparable with the reported value $\rho = 0.94$ obtained for SHG from a ML WS_2 coupled to a passive photonic structure.[25]

Next, we compare the efficiency of SHG from polaritons with a ML WS_2 that was transferred on 300 nm thermal oxide on silicon. WS_2 was chosen as an archetypal ML, as it has one of the largest values of second-order permittivity. The power-dependent measurements in Figure 3b show the ratio between the SHG signal from the WSe_2 self-hybridized polariton sample and a reference WS_2 ML that is pumped at the same wavelength. The plot can be divided into three distinct regimes of power. At low pump powers (region I) it can be seen that the efficiency of SHG from the polariton system is higher than the one from a non-centrosymmetric ML WS_2 sample. At intermediate powers (region II) of ≈1 mW, there is a drop in the ratio of intensities of SHG generation in the polariton systems and the ML WS_2. This is the region where the Kerr-like polariton nonlinearity via phase space filling of the excitons kicks in. At higher pump powers (region III), as a consequence of phase space filling, the lower polaritons branch shifts toward higher energies, thereby making the pump laser detuned from the lower polariton resonance. This results in overall reduction in efficiency, as shown in Figure 3b. This effect results in a deviation from the typical slope of 2 for the SHG signal from the polariton system (Figure S2a and Supporting Information, Note 4.) Individual plots for SHG intensity comparison for the self-hybridized polaritons and ML WS_2 as a function of pump

https://doi.org/10.1021/acsphotonics.1c01242
ACS Photonics 2022, 9, 503−510

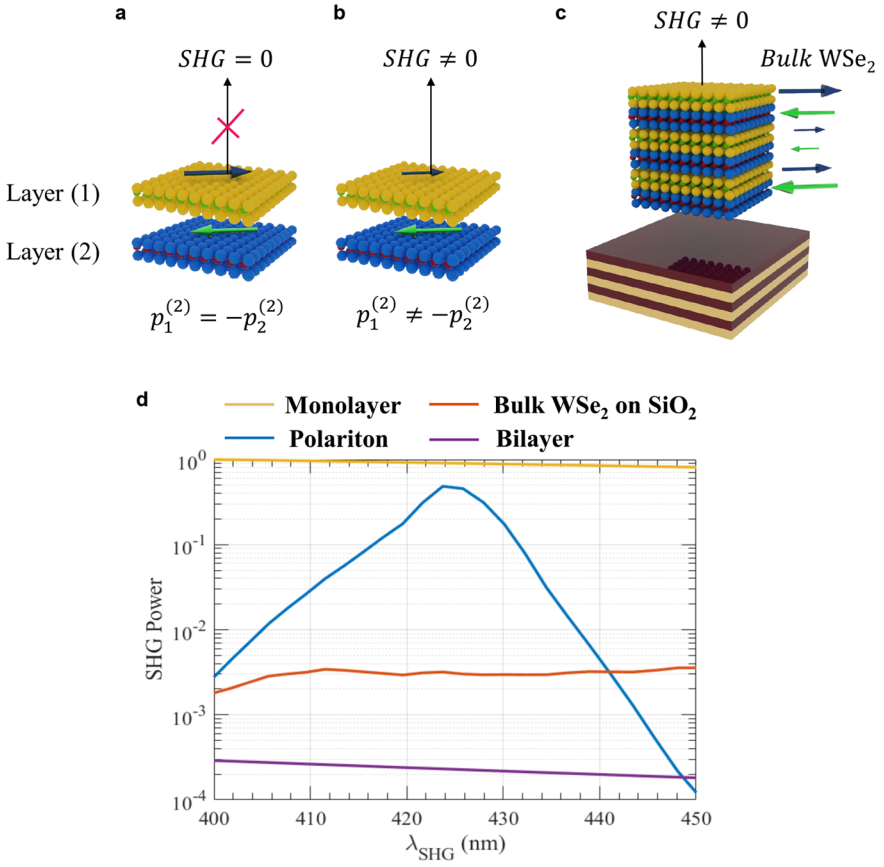

Figure 4. (a) 2H stacked bilayer WSe_2 with equal second-order nonlinear polarization p and out-of-phase, hence, generating no SHG. (b) 2H stacked bilayer WSe_2 with unequal and opposite p can generate nonzero SHG. (c) Enhancing the nonlinear polarization in bulk WSe_2 by coupling to a photonic cavity where the fundamental field significantly increases, along with unequal second-order polarization from individual layers in the bulk TMDC. (d) Normalized SHG power calculated for the structures in (c) with a bulk TMDC height of 140 nm. The ratios of the SHG at the SH wavelength 425 nm are 0.9:0.5:0.003:0.0002 for the ML, polariton system, bulk on SiO_2, and bilayer, respectively.

power are shown in Figure S6. Such phase space filling effects have been extensively studied in various ML TMDC systems with interest in the generation of polariton blockade.[36−40] A detailed study of this third-order nonlinearity is beyond the scope of this work.

We now examine the physical processes that give rise to such intense SHG from a centrosymmetric material. One could posit that the SHG is generated from an odd layered system with the last layer generating an intense SHG owing to loss of inversion symmetry. However, this would result in a broadband response of the SHG and not be limited to the polariton resonance, as shown in Figure 2b. Moreover, this strong fundamental wavelength dependence has been noted in several TMDC flakes of various thicknesses when they are pumped on and off the polariton resonance. Another possibility is the enhancement of the residual surface SHG rate due to an enhanced density of photonic states owing to a cavity mode that is resonant with either the SH or the fundamental wavelength. To investigate this possibility, we perform FDTD simulations for a bulk material with a fixed $\chi^{(2)}$ using a broadband fundamental source, where we replicate the configuration used in our experiment and obtain an enhancement of ≈16×. See Supporting Information, Note 5 and Figure S4b for more details. A similar enhancement has been reported in systems where a ML TMDC flake is coupled to passive resonant structures.[24−26] This passive enhancement factor, however, fails to explain the drastic enhancement of at least 3 orders of magnitude when the system is excited at the polariton resonance. To fully explain the experimental results, we use a model with layers of alternating $\chi^{(2)}$,[15] and we set the value of $\chi^{(2)}$ to be 4×10^{-9} nm/V. Any crystal with inversion symmetry should possess zero second-order nonlinearity because the macroscopic polarization, $p^{(2)}(E) = -p^{(2)}(-E)$ leads to the vanishing of all even nonlinear susceptibility under the electric dipole approximation. This is indeed true for 2H stacking of an even number of layers in 2D TMDCs in which the inversion symmetry is restored. This cancellation of SHG for an even number of layers can be envisioned macroscopically, as shown in Figure 4a, where two successive MLs have alternative signs of the induced second-order polarization, that is, $\chi^{(2)}$ in the first layer is equivalent to $-\chi^{(2)}$ in the next layer, leading to a canceling of the SHG for an even number of layers in the far field. However, recent reports have shown that, despite the existence of geometrical inversion symmetry in some systems, for example, bilayer WSe_2, SHG can arise by breaking the inversion symmetry of the induced charges. If the field is asymmetric across different layers of the 2D TMDC, the nonlinear polarizations add coherently, generating SHG. This is depicted in Figure 4b, where the nonlinear polarizations represented by arrows are in opposite directions, but not of the same magnitude.[41] Recent work has additionally shown that artificially stacking 2D layers with a controllable twist angle

https://doi.org/10.1021/acsphotonics.1c01242
ACS Photonics 2022, 9, 503−510

between the layers can lead to enhancing or suppressing SHG, described by a superposition relation shown in Figure 4b, but with the arrows now pointing along different directions.[42] For the given polariton system, if we consider a pump wavelength at the fundamental frequency ω impinging from the top, the electric field distribution is not symmetric. In this case, the SHG from different layers does not cancel each other in the far field, as shown in Figure 4c, thereby resulting in the SHG signal that is observed in the experiment. This effect is further enhanced by the higher photonic density of states at the polariton branches. While this model captures the qualitative behavior of the SHG, it overestimates the value of the SHG response shown previously in a related work.[15] We classically model the enhancement in the nonlinear process by solving coupled linear equations at the fundamental frequency ω and at the SHG frequency 2ω. To describe the SHG response of the system, we model the WSe_2 as a mutlilayer system with a layer thickness of 0.5 nm. The only nonvanishing susceptibility terms are

$$\chi^{(2)}_{yyy} = -\chi^{(2)}_{yxx} = \chi^{(2)}_{xxy} = \chi^{(2)}_{xyx} \quad (1)$$

where y is the armchair direction of the crystal lattice. We assume in the simulation that the incident polarization is aligned with the armchair direction, giving rise only to SHG polarized in the armchair direction. We model the nonlinear polarization in each layer as

$$p^{(2)}_l = \epsilon_0 \chi^{(2)}_{l,yyy} E^{(\omega)2}_{l,y} \quad (2)$$

where l is the layer number, $\chi^{(2)}_l$ is positive for odd layers and negative for even layers counted from a fixed reference, and $E^{(\omega)}_{l,y}$ is the field distribution in layer l at the fundamental frequency. We then use this polarization current as the source for the SH signal. We use this model to describe the SHG from a ML and the polariton system. Interestingly, using this simple model, we can observe an enhancement of around 4 orders of magnitude between SHG from ML and the SHG from the bilayer, which perfectly matches our experimental results. The polariton system shows enhanced SHG at lower polariton resonance with a SHG efficiency close to that of a ML. We attribute this large SHG in the cavity coupled system near resonance due to the combination of the field enhancement and its spatial profile, which leads to an asymmetric distribution of nonlinear polarization. At the same time, in bulk WSe_2 outside the lower polariton resonance, we found an almost negligible SHG owing to the near perfect cancellation of the SH field of individual layers in the far field, as shown in Figure 4d.

The model used here does not invoke nonlocal effects and remains well within the dipole approximation. The analysis shows that in layered systems like TMDCs, SHG should be treated as a collective effect of its constituent noncentrosymmetric ML.

Finally, we comment on the advantages of having a dielectric spacer layer. In the structure described in the text above, the use of air as a spacer layer allowed us to access narrower polariton modes in addition to the advantages mentioned earlier. However, similar SHG responses can also be found in structures with PMMA spacers and a metal mirror. The resonances obtained in those systems are broader and have a lower enhancement due to their lower quality factor. We could do away with the bottom mirror and form self-hybridized polaritons in bulk TMDCs on glass or silicon substrates as reported in several works.[9,28] However, in these systems we are limited to bulks of thickness ranging only about from about 60 to 100 nm. This is shown via various transfer matrix calculation for different device geometries in the Supporting Information, Note 6 and Figure S5. We also note that a similar analysis can be done to explain the weak bulk SHG observed in ref 28 in bulk TMDCs in a narrow range of thickness. Strong SHG seen in self-hybridized polariton systems with poly(methyl methacrylate) (PMMA) spacer is shown in Supporting Information, Note 8 and Figure S7.

In summary, here we have demonstrated a platform to relax crystal symmetry requirements for second-order nonlinear response in bulk TMDC crystals via formation of exciton polaritons. The fact that we achieve strong nonlinear responses in bulk TMDCs reduces challenges with fabrication and integration into passive photonic platforms. Although we focus solely on the SHG process in the current work, other $\chi^{(2)}$ processes, like sum/difference frequency generation and optical parametric amplification, can be explored in these systems. In addition, these polariton systems inherently possess a $\chi^{(3)}$ response that can lead to saturation of absorption, tunable index of refraction and single photon nonlinearity via polariton blockade, thereby forming a versatile platform for a plethora of applications in the field of nonlinear photonics and quantum optics. Furthermore, the power-dependent saturation of the SHG can be used to estimate polariton−polariton interaction strengths in systems where traditional techniques of measuring contrasts in resonant laser reflection as a function of power are not feasible.

METHODS

A DBR with center wavelength of 740 nm consisting of 10.5 periods of alternating TiO_2 and SiO_2 with thicknesses of 88 nm and 128 m, respectively, was sputtered on a glass substrate, with SiO2 being the top layer. A 7.5 μm by 7.5 μm square hole was written with electron beam lithography (Elionix ELS G100) on a spin-coated positive electron beam resist (495PMMA A6) of thickness 440 nm. A bulk WSe_2 crystal of 140 nm thickness and size of 60 × 70 μm^2 was exfoliated with the scotch tape method and transferred onto the square hole via the polypropylene carbonate (PPC) transfer technique in order to create the free-standing WSe_2.[1] In order to remove residue left by the PPC process, the structure was then soaked in chloroform for 2 h at room temperature. The thicknesses of both the air hole and the WSe_2 were measured with atomic force microscopy (Bruker Dimension FastScan). White light dispersion data was collected by using a broadband halogen light source and imaging the back aperture of a 50× objective with a numerical aperture of 0.8 (Olympus MPLFLN) onto a Princeton Instruments Monochromator with an EMCCD Camera (Pixis 1024B).

For the SHG measurements, a titanium−sapphire laser (Coherent Mira) was used to pump at the fundamental wavelength of 832 nm, while the SHG signal was detected through the Princeton Instruments Monochromator. A 500 nm short pass filter was used in the collection side to filter out the excitation beam. Linear polarization measurements were recorded by using a linear polarizer (LP) in the excitation path and a collinear LP in the collection path. For helicity-resolved SHG measurements, the excitation circular polarization was determined by using a LP followed by a quarter-wave plate (QWP) to determine the left and right circularly polarized states of the excitation beam. In the collection path,

https://doi.org/10.1021/acsphotonics.1c01242
ACS Photonics 2022, 9, 503−510

an analyzer of a QWP followed by an LP was used to resolve the chiral response of the system.

Coupled Mode Theory. In this work, the nonlinear response of bulk WSe_2 is underpinned by coupling it to a photonic cavity in the form of a Fabry−Perot resonator with its two reflective surfaces, which are a bulk WSe_2 and the DBR, as shown in Figure 1a. The system represents two eigenmodes, represented by their respective frequencies ω_a and ω_b. Here, ω_a represents the exciton resonance of the WSe_2, and ω_b represents the resonance frequency of the photonic cavity which can be actively tuned with changing its height h. For an external excitation, the photonic cavity mode is indirectly excited, and the bulk WSe_2 mode is excited directly from an impinging wave, as shown in Figure 1a. These dynamics can be captured by employing the coupled mode theory (CMT) to describe the coupled oscillators system. The two oscillators are the material resonance ω_a and the photonic cavity mode ω_b. The material resonance mode is coupled to the radiation incident from above with radiation rate γ_r, while the cavity mode is coupled indirectly to the incident radiation. The two modes are coupled with coupling rate κ thus forming the half matter half-light particles when $\kappa > \gamma_r$. The CMT governing equations are

$$\frac{da}{dt} = (i\omega_a - \gamma_a - \gamma_r)a + i\kappa b + \sqrt{2\gamma_r}s_+ \tag{3}$$

$$s_- = -s_+ + \sqrt{2\gamma_r}a \tag{4}$$

$$\frac{db}{dt} = (i\omega_b - \gamma_b)b + i\kappa a \tag{5}$$

where γ_a and γ_b are the absorption rates of the 2D TMDC, and the photonic cavity respectively while γ_r is the radiative coupling rate. For oblique incidence, the material resonance ω_a does not change, the cavity resonance changes as

$$\omega_b^2 = \omega_{b0}^2 + c^2k_\perp^2 \rightarrow \omega_b \approx \omega_{b0} + 0.5\sin^2\theta \tag{6}$$

with c representing the light speed and $k_\perp$ representing the normal wavenumber inside the cavity. We can solve the differential equations under slowly varying approximation and give the reflection as

$$R = \left|\frac{-(i\Delta\omega_a + \gamma_a + \gamma_r)(i\Delta\omega_b + \gamma_b) - \kappa^2 + 2\gamma_r(i\Delta\omega_b + \gamma_b)}{(i\Delta\omega_a + \gamma_a + \gamma_r)(i\Delta\omega_b + \gamma_b) + \kappa^2}\right|^2 \tag{7}$$

Here, $\omega_{b0} = 2.23 \times 10^{15}$ rad/s, $\omega_a = 2.55 \times 10^{15}$ rad/s, $\gamma_a = 0.015\omega_b$, $\gamma_b = 0.001\ 1\omega_a$, $\gamma_r = 0.05\omega_a$, $\kappa = 0.004\omega_b$, calculated to match the experimental results.

Full Wave Analysis of Second-Order Polarization. In the simulation model we use the undepleted pump approximation due to the known low conversion efficiency, confirmed by the measurement as well. In the model, we solve two coupled frequency domain problems. The two problems have the same geometry with different excitation sources. The source in the first problem is the pump excitation at frequency, ω_0, and we solve for the fields in all regions due to that pump. Once solved, this field generates alternating nonlinear polarization currents in the WSe_2 region, which will be used as the source for the second problem at frequency $2\omega_0$. The second-order polarization current is a superposition of the nonlinear polarization current generated by the pump, and the additional polarization that exists due to the permittivity of the WSe_2 (if in vacuum no such linear polarization current exists, and the total polarization will be only due to the nonlinear susceptibility). This causes the net second-order polarization to lose the alternating behavior acquired from the of the nonlinear polarization current in the region of the field asymmetry and instead be in phase. See Supporting Information, Note 9 and Figure S8 for more details.

■ ASSOCIATED CONTENT

Supporting Information

The Supporting Information is available free of charge at https://pubs.acs.org/doi/10.1021/acsphotonics.1c01242.

Transfer matrix simulations and electric field distribution, SHG characterization, SH electric field patterns as a function of linear polarization, carrier-induced excitonic nonlinearity, calculation of Purcell enhancement due to formation of self-hybridized polaritons, self-hybridized polaritons in various geometries, comparison of the power-dependent intensity of self-hybridized polaritons and ML WS_2, SHG from self-hybridized polaritons in bulk $MoSe_2$ on DBR, and full wave analysis of the SHG process (PDF)

■ AUTHOR INFORMATION

Corresponding Author

Vinod M Menon − *Department of Physics, The Graduate Center, City University of New York, New York, New York 10016, United States; Department of Physics, City College of New York, City University of New York, New York, New York 10031, United States;* orcid.org/0000-0002-9725-6445; Email: vmenon@ccny.cuny.edu

Authors

Mandeep Khatoniar − *Department of Physics, The Graduate Center, City University of New York, New York, New York 10016, United States; Department of Physics, City College of New York, City University of New York, New York, New York 10031, United States*

Rezlind Bushati − *Department of Physics, The Graduate Center, City University of New York, New York, New York 10016, United States; Department of Physics, City College of New York, City University of New York, New York, New York 10031, United States*

Ahmed Mekawy − *Photonics Initiative, Advanced Science Research Center, City University of New York, New York, New York 10031, United States; Department of Electrical Engineering, City College of New York, City University of New York, New York, New York 10031, United States*

Florian Dirnberger − *Department of Physics, City College of New York, City University of New York, New York, New York 10031, United States*

Andrea Alù − *Department of Physics, The Graduate Center, City University of New York, New York, New York 10016, United States; Department of Electrical Engineering, City College of New York, City University of New York, New York, New York 10031, United States; Photonics Initiative, Advanced Science Research Center, City University of New York, New York, New York 10031, United States;* orcid.org/0000-0002-4297-5274

Complete contact information is available at: https://pubs.acs.org/10.1021/acsphotonics.1c01242

Author Contributions

M.K., R.B., and V.M. conceived the idea, M.K. and R.B. performed the experiments, A.M. and A.A. performed theoretical and computational studies, and V.M. supervised the experiment. All authors contributed to writing the manuscript.

Funding

Authors acknowledge DARPA Nascent Light–Matter Interactions program, ARO MURI (W911NF-17-1-0312) and Simons Foundation for support. The devices were fabricated at the Nanofabrication facilities at the ASRC, CUNY.

Notes

The authors declare no competing financial interest.

■ ACKNOWLEDGMENTS

We thank Professor Wang Yao from The University of Hong Kong for useful discussions. Raw data and analysis codes used in this manuscript are freely available upon reasonable request.

■ REFERENCES

(1) Mak, K. F.; Lee, C.; Hone, J.; Shan, J.; Heinz, T. F. Atomically thin MoS_2: A new direct-gap semiconductor. *Phys. Rev. Lett.* **2010**, *105*, 2−5.
(2) Zeng, H.; Liu, G. B.; Dai, J.; Yan, Y.; Zhu, B.; He, R.; Xie, L.; Xu, S.; Chen, X.; Yao, W.; Cui, X. Optical signature of symmetry variations and spin-valley coupling in atomically thin tungsten dichalcogenides. *Sci. Rep.* **2013**, *3*, 2−6.
(3) Wang, G.; Chernikov, A.; Glazov, M. M.; Heinz, T. F.; Marie, X.; Amand, T.; Urbaszek, B. Colloquium: Excitons in atomically thin transition metal dichalcogenides. *Rev. Mod. Phys.* **2018**, *90*, 021001.
(4) Xiao, D.; Liu, G.-B.; Feng, W.; Xu, X.; Yao, W. Coupled Spin and Valley Physics in Monolayers of MoS_2 and Other Group-VI Dichalcogenides. *Phys. Rev. Lett.* **2012**, *108*, 196802.
(5) Liu, X.; Galfsky, T.; Sun, Z.; Xia, F.; Lin, E. C.; Lee, Y. H.; Kéna-Cohen, S.; Menon, V. M. Strong light-matter coupling in two-dimensional atomic crystals. *Nat. Photonics* **2015**, *9*, 30−34.
(6) Sun, Z.; Gu, J.; Ghazaryan, A.; Shotan, Z.; Considine, C. R.; Dollar, M.; Chakraborty, B.; Liu, X.; Ghaemi, P.; Kéna-Cohen, S.; Menon, V. M. Optical control of room-temperature valley polaritons. *Nat. Photonics* **2017**, *11*, 491−496.
(7) Chen, Y.-J.; Cain, J. D.; Stanev, T. K.; Dravid, V. P.; Stern, N. P. Valley-polarized exciton−polaritons in a monolayer semiconductor. *Nat. Photonics* **2017**, *11*, 431−435.
(8) Dufferwiel, S.; Lyons, T. P.; Solnyshkov, D. D.; Trichet, A. A. P.; Withers, F.; Schwarz, S.; Malpuech, G.; Smith, J. M.; Novoselov, K. S.; Skolnick, M. S.; Krizhanovskii, D. N.; Tartakovskii, A. I. Valley-addressable polaritons in atomically thin semiconductors. *Nat. Photonics* **2017**, *11*, 497−501.
(9) Munkhbat, B.; Baranov, D. G.; Stührenberg, M.; Wersäll, M.; Bisht, A.; Shegai, T. Self-Hybridized Exciton-Polaritons in Multilayers of Transition Metal Dichalcogenides for Efficient Light Absorption. *ACS Photonics* **2019**, *6*, 139−147.
(10) Gogna, R.; Zhang, L.; Deng, H. Self-Hybridized, Polarized Polaritons in ReS2 Crystals. *ACS Photonics* **2020**, *7*, 3328−3332.
(11) Verre, R.; Baranov, D. G.; Munkhbat, B.; Cuadra, J.; Käll, M.; Shegai, T. Transition metal dichalcogenide nanodisks as high-index dielectric Mie nanoresonators. *Nat. Nanotechnol.* **2019**, *14*, 679−683.
(12) Kumar, N.; Najmaei, S.; Cui, Q.; Ceballos, F.; Ajayan, P. M.; Lou, J.; Zhao, H. Second harmonic microscopy of monolayer MoS2. *Phys. Rev. B: Condens. Matter Mater. Phys.* **2013**, *87*, 1−6.
(13) Malard, L. M.; Alencar, T. V.; Barboza, A. P. M.; Mak, K. F.; De Paula, A. M. Observation of intense second harmonic generation from MoS2 atomic crystals. *Phys. Rev. B: Condens. Matter Mater. Phys.* **2013**, *87*, 1−5.
(14) Wagoner, G. A.; Persans, P. D.; Van Wagenen, E. A.; Korenowski, G. M. Second-harmonic generation in molybdenum disulfide. *J. Opt. Soc. Am. B* **1998**, *15*, 1017.
(15) Li, Y.; Rao, Y.; Mak, K. F.; You, Y.; Wang, S.; Dean, C. R.; Heinz, T. F. Probing Symmetry Properties of Few-Layer MoS2 and h-BN by Optical Second-Harmonic Generation. *Nano Lett.* **2013**, *13*, 3329−3333.
(16) Alexeev, E. M.; et al. Resonantly hybridized excitons in moiré superlattices in van der Waals heterostructures. *Nature* **2019**, *567*, 81−86.
(17) Seyler, K. L.; Rivera, P.; Yu, H.; Wilson, N. P.; Ray, E. L.; Mandrus, D. G.; Yan, J.; Yao, W.; Xu, X. Signatures of moiré-trapped valley excitons in MoSe2/WSe2 heterobilayers. *Nature* **2019**, *567*, 66−70.
(18) Tran, K.; et al. Evidence for moiré excitons in van der Waals heterostructures. *Nature* **2019**, *567*, 71−75.
(19) Jin, C.; Regan, E. C.; Yan, A.; Iqbal Bakti Utama, M.; Wang, D.; Zhao, S.; Qin, Y.; Yang, S.; Zheng, Z.; Shi, S.; Watanabe, K.; Taniguchi, T.; Tongay, S.; Zettl, A.; Wang, F. Observation of moiré excitons in WSe2/WS2 heterostructure superlattices. *Nature* **2019**, *567*, 76−80.
(20) Yao, K.; Yanev, E.; Chuang, H. J.; Rosenberger, M. R.; Xu, X.; Darlington, T.; McCreary, K. M.; Hanbicki, A. T.; Watanabe, K.; Taniguchi, T.; Jonker, B. T.; Zhu, X.; Basov, D. N.; Hone, J. C.; Schuck, P. J. Continuous Wave Sum Frequency Generation and Imaging of Monolayer and Heterobilayer Two-Dimensional Semiconductors. *ACS Nano* **2020**, *14*, 708−714.
(21) Trovatello, C.; Marini, A.; Xu, X.; Lee, C.; Liu, F.; Curreli, N.; Manzoni, C.; Dal Conte, S.; Yao, K.; Ciattoni, A.; Hone, J.; Zhu, X.; Schuck, P. J.; Cerullo, G. Optical parametric amplification by monolayer transition metal dichalcogenides. *Nat. Photonics* **2021**, *15*, 6−10.
(22) Dinparasti Saleh, H.; Vezzoli, S.; Caspani, L.; Branny, A.; Kumar, S.; Gerardot, B. D.; Faccio, D. Towards spontaneous parametric down conversion from monolayer MoS_2. *Sci. Rep.* **2018**, *8*, 3862.
(23) Wen, X.; Gong, Z.; Li, D. Nonlinear optics of two-dimensional transition metal dichalcogenides. *InfoMat* **2019**, *1*, 317−337.
(24) Fryett, T. K.; Seyler, K. L.; Zheng, J.; Liu, C.-H.; Xu, X.; Majumdar, A. Silicon photonic crystal cavity enhanced second-harmonic generation from monolayer WSe 2. *2D Mater.* **2017**, *4*, 015031.
(25) Hu, G.; Hong, X.; Wang, K.; Wu, J.; Xu, H.-X.; Zhao, W.; Liu, W.; Zhang, S.; Garcia-Vidal, F.; Wang, B.; Lu, P.; Qiu, C.-W. Coherent steering of nonlinear chiral valley photons with a synthetic Au−WS2 metasurface. *Nat. Photonics* **2019**, *13*, 467−472.
(26) Chen, H.; Corboliou, V.; Solntsev, A. S.; Choi, D.-Y.; Vincenti, M. A.; de Ceglia, D.; de Angelis, C.; Lu, Y.; Neshev, D. N. Enhanced second-harmonic generation from two-dimensional MoSe2 on a silicon waveguide. *Light: Sci. Appl.* **2017**, *6*, No. e17060.
(27) Li, C.; Lu, X.; Srivastava, A.; Storm, S. D.; Gelfand, R.; Pelton, M.; Sukharev, M.; Harutyunyan, H. Second Harmonic Generation from a Single Plasmonic Nanorod Strongly Coupled to a WSe2Monolayer. *Nano Lett.* **2021**, *21*, 1599−1605.
(28) Busschaert, S.; Reimann, R.; Cavigelli, M.; Khelifa, R.; Jain, A.; Novotny, L. Transition Metal Dichalcogenide Resonators for Second Harmonic Signal Enhancement. *ACS Photonics* **2020**, *7*, 2482−2488.
(29) Choudhury, B. D.; Sahoo, P. K.; Sanatinia, R.; Andler, G.; Anand, S.; Swillo, M. Surface second harmonic generation from silicon pillar arrays with strong geometrical dependence. *Opt. Lett.* **2015**, *40*, 2072−2075.
(30) Bhowmik, G.; An, Y. Q.; Schujman, S.; Diebold, A. C.; Huang, M. Optical second harmonic generation from silicon (100) crystals with process tailored surface and embedded silver nanostructures for silicon nonlinear nanophotonics. *J. Appl. Phys.* **2020**, *128*, 165106.
(31) Lu, X.; Moille, G.; Rao, A.; Westly, D. A.; Srinivasan, K. Efficient photoinduced second-harmonic generation in silicon nitride photonics. *Nat. Photonics* **2021**, *15*, 131−136.

https://doi.org/10.1021/acsphotonics.1c01242
ACS Photonics 2022, 9, 503−510

(32) Makarov, S. V.; Petrov, M. I.; Zywietz, U.; Milichko, V.; Zuev, D.; Lopanitsyna, N.; Kuksin, A.; Mukhin, I.; Zograf, G.; Ubyivovk, E.; Smirnova, D. A.; Starikov, S.; Chichkov, B. N.; Kivshar, Y. S. Efficient Second-Harmonic Generation in Nanocrystalline Silicon Nanoparticles. *Nano Lett.* **2017**, *17*, 3047−3053.
(33) Carusotto, I.; Ciuti, C. Quantum fluids of light. *Rev. Mod. Phys.* **2013**, *85*, 299−366.
(34) Li, D.; Xiong, W.; Jiang, L.; Xiao, Z.; Rabiee Golgir, H.; Wang, M.; Huang, X.; Zhou, Y.; Lin, Z.; Song, J.; Ducharme, S.; Jiang, L.; Silvain, J.-F.; Lu, Y. Multimodal Nonlinear Optical Imaging of MoS2 and MoS2-Based van der Waals Heterostructures. *ACS Nano* **2016**, *10*, 3766−3775.
(35) Tang, C. L.; Rabin, H. Selection Rules for Circularly Polarized Waves in Nonlinear Optics. *Phys. Rev. B* **1971**, *3*, 4025−4034.
(36) Verger, A.; Ciuti, C.; Carusotto, I. Polariton quantum blockade in a photonic dot. *Phys. Rev. B* **2006**, *73*, 193306.
(37) Tan, L. B.; Cotlet, O.; Bergschneider, A.; Schmidt, R.; Back, P.; Shimazaki, Y.; Kroner, M.; İmamoğlu, A. m. c. Interacting Polaron-Polaritons. *Phys. Rev. X* **2020**, *10*, 021011.
(38) Zhang, L.; Wu, F.; Hou, S.; Zhang, Z.; Chou, Y.-H.; Watanabe, K.; Taniguchi, T.; Forrest, S. R.; Deng, H. Van der Waals heterostructure polaritons with moiré-induced nonlinearity. *Nature* **2021**, *591*, 61−65.
(39) Barachati, F.; Fieramosca, A.; Hafezian, S.; Gu, J.; Chakraborty, B.; Ballarini, D.; Martinu, L.; Menon, V.; Sanvitto, D.; Kéna-Cohen, S. Interacting polariton fluids in a monolayer of tungsten disulfide. *Nat. Nanotechnol.* **2018**, *13*, 906−909.
(40) Gu, J.; Walther, V.; Waldecker, L.; Rhodes, D.; Raja, A.; Hone, J. C.; Heinz, T. F.; Kéna-Cohen, S.; Pohl, T.; Menon, V. M. Enhanced nonlinear interaction of polaritons via excitonic Rydberg states in monolayer WSe2. *Nat. Commun.* **2021**, *12*, 2269.
(41) Yu, H.; Talukdar, D.; Xu, W.; Khurgin, J. B.; Xiong, Q. Charge-Induced Second-Harmonic Generation in Bilayer WSe2. *Nano Lett.* **2015**, *15*, 5653−5657.
(42) Hsu, W.-T.; Zhao, Z.-A.; Li, L.-J.; Chen, C.-H.; Chiu, M.-H.; Chang, P.-S.; Chou, Y.-C.; Chang, W.-H. Second Harmonic Generation from Artificially Stacked Transition Metal Dichalcogenide Twisted Bilayers. *ACS Nano* **2014**, *8*, 2951−2958.

https://doi.org/10.1021/acsphotonics.1c01242
ACS Photonics 2022, 9, 503−510